Supplementary: VCSEL–Metasurface OAM Transmitters for High-Capacity Optical Wireless Links

Rizwana Ahmad[1*†], Arttu Nieminen[2†], Isaac N. O. Osahon[1], Iman Tavakkolnia[1], Humeyra Caglayan[2,3], Harald Haas[1]

[1]LiFi Research and Development Centre, Electrical Engineering Division, University of Cambridge, Cambridge, UK.
[2]Physics Department, Photonics Unit, Tampere University, Tampere, Finland.
[3]Electrical Engineering, Photonic Integration, Eindhoven University of Technology, Eindhoven, Netherlands.

*Corresponding author(s). E-mail(s): ra714@cam.ac.uk;
†These authors contributed equally to this work.

S1 Summary of related works

Previous orbital angular momentum (OAM) generation approaches have predominantly relied on bulky free-space components such as spatial light modulators and spiral phase plates [1–3, 6–8], externally pumped and costly laser architectures [9–13], or complex coherent modulation schemes [1–3, 10–12, 14], all of which limit scalability and system-level integration. Moreover, most reported demonstrations operate exclusively at the 850 nm [4, 5] or 1550 nm wavelength. In contrast, to the best of our knowledge, this work presents the first 1310 nm vertical cavity surface emitting laser (VCSEL)–metasurface hybrid platform for OAM generation, with additional experimental validation at 1550 nm, thereby encompassing both major telecommunication bands. While the current implementation is hybrid, it paves the way toward fully monolithic integration, providing a pathway to low-cost, compact, and energy-efficient OAM emitters suitable for large-scale optical wireless communication and photonic-integrated systems. Table S1 summarizes the releated works.

Table S1 Comparative overview of relevant literature on orbital angular momentum (OAM)-based optical wireless communication (OWC) systems. This table summarizes key parameters including wavelength (λ), data rate (R), bandwidth (B), number of OAM modes, total number of wavelength division multiplexing (WDM) and ploarization dvision mulitplexing (PDM) channels (N_{WDM}, N_{PDM}), normalized spectral efficiency (η), and the use of intensity modulation and direct detection (DD), metasurfaces (M), and VCSELs (V). The final row highlights the unique contributions of the present work, particularly the combination of a 1310 nm VCSEL with a metasurface and its broadband operation. Our work considers the BER threshold of < 5.6 x 10^{-2} specified by LTE system requirements.

Ref.	λ (nm)	R (Gbps)	B (GHz)	OAM	N_{WDM}, N_{PDM}	η (bps/Hz)	DD	**M**	V	Notes
[1]	1550	1370	50	2	4	3.2	✗	✗	–	Spatial light modulators (SLMs)
[2]	1500	120	30	4	–	4.0	✗	✗	–	Vortex HWP, turbulence
[3]	1550	80	10	2	–	2.0	✗	✗	✗	2×2 MIMO equalization, SLMs
[4]	850	10	7	1	–	1.4	✓	✗	✓	1.5 m FSO + 3 m MMF; NRZ–OOK; single OAM mode
[5]	850	40	10	4	–	1	✓	✗	✓	4 OAM channels; low-cost VCSEL array; spatial multiplexing
[6]	∼1550	2000	–	2	25	–	✓	✗	–	SLMs
[7]	1550	1440	40	12	2	1.5	✓	✗	✗	ECL, SLM
[8]	1550	39.06	9.76	3	–	1.33	✓	✗	–	SLM, diversity, turbulence
[9]	405–686	805	–	10	8	–	✓	✗	✗	Octa-laser, APD
[10]	∼1550	448	–	4	2	–	✗	✓	✗	Multichannel OAM, ECL, gold antenna, ICR
[11]	1550	1560	–	4	4, 2	–	✗	✓	✗	Metallic metasurface for demux, CW laser
[12]	1550	2730	–	4	7, 2	–	✗	✓	✗	PBM metasurfaces, CW laser
[13]	1064, 520	40	-	4	-	-	✓	✓	✗	underwater, diferactive phase metasurface
[14]	1550	200	–	2	–	–	✗	✗	–	Genetic algorithm to reduce crosstalk
This work	1310, 1550	32.57	5.8	2	–	2.81	✓	✓	✓	Propagation phase metasurface, PIN PD, first 1310 nm VCSEL–metasurface integration, broadband operation

S2 Scalability of OAM Modes and Data Rates

In our experiments, OAM transmission was demonstrated using only two modes ($\ell = 1$ and $\ell = 2$), limited by fabrication yield and available test equipment. To evaluate scalability, we performed simulations for ten modes ($\ell = \pm 1$ to ± 5) at both 1310 and 1550 nm (Fig. S1 and S2).

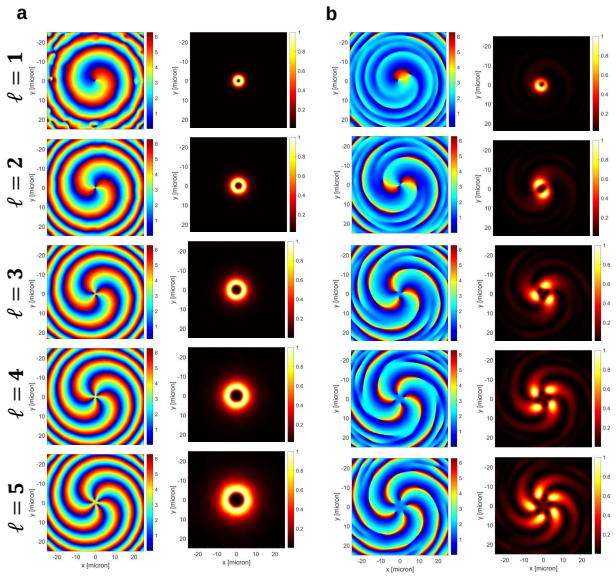

Fig. S1 Phase and intensity distributions of positive OAM modes. a, Simulated phase (left) and intensity (right) profiles for OAM modes with topological charges $\ell = 1$ to 5 at 1310 nm. **b**, Corresponding phase and intensity profiles at 1550 nm.

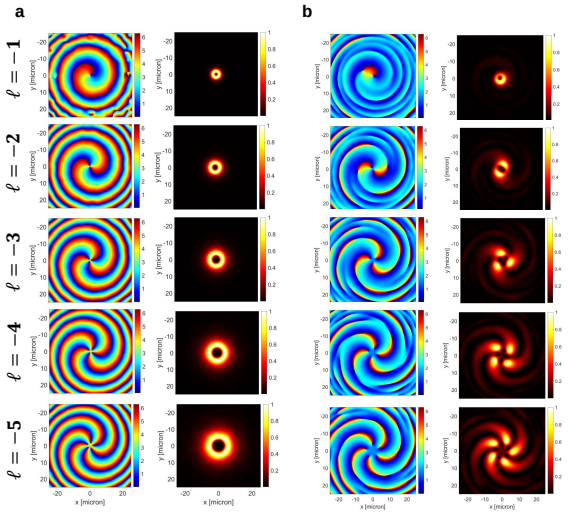

Fig. S2 Phase and intensity distributions of negative OAM modes. a, Simulated phase (left) and intensity (right) profiles for OAM modes with topological charges $\ell = -1$ to -5 at 1310 nm. **b**, Corresponding phase and intensity profiles at 1550 nm.

At the design wavelength of 1310 nm, the simulated beams retain clean, donut-shaped intensity distributions and spiral phase distributions across all charges, with

negligible distortions. By contrast, at 1550 nm, the phase response becomes chromatically detuned, leading to asymmetric ring patterns and residual Gaussian ($\ell = 0$) components. Mode purity analysis (Fig. S3a) confirms this trend: all charges maintain purity above 90% within a broad 100 nm window (1280 nm–1380 nm), whereas purity decreases nearly linearly from ∼80% to ∼60% across the 1450–1550 nm band due to incomplete phase compensation. This leakage manifests as weak $\ell = 0$ intensity in the far field (Fig. S3b, left).

Experimentally, the system achieved per-channel data rates of 16 Gbps at 1310 nm and 13 Gbps at 1550 nm, both corresponding to the LTE forward-error-correction limit reported in Fig. 3b of the main article. Although only $\ell = 1$ and $\ell = 2$ were experimentally verified, due to fabrication yield and measurement hardware constraints, the close agreement between measurements and simulations indicates that the metasurface–VCSEL platform can be extended to higher-order modes. By extrapolating the number of supported modes, a ten-mode configuration ($\ell = \pm1$ to ±5) is projected to achieve aggregate throughputs exceeding 160 Gbps (10×16 Gbps) at 1310 nm and 130 Gbps (10×13 Gbps) at 1550 nm. These findings demonstrate that a compact, low-cost, and energy-efficient integrated system can deliver ultra-high data rates, providing a scalable alternative to previously reported Tbps-range OAM-WDM/PDM systems that rely on bulky and costly free-space optics or external lasers [1–3, 6–8, 13–16]. Beyond high-capacity optical wireless communication, such integrated OAM sources open avenues for short-reach data interconnects, OWC access points, secure quantum key distribution, precision imaging, and advanced optical sensing, where compactness, manufacturability, and energy efficiency are as critical as datarate.

S3 Experimental Setup

For completeness, Fig. S4 presents the schematic of the experimental setup, reproduced from Fig. 3a of the main text, while Fig. S5 shows a photograph of the actual implementation.

On the transmitter side, we have used a) 1310 nm VCSEL (Optilab VCSEL-1310-SM) or b) 1550 nm (Thorlabs LPSC-1550-FC) as the optical source. The optical sources were DC-biased using a Keysight E36313A power supply to ensure linear optical modulation. The 1310 nm VCSEL was biased at 1.85 V with a driving current of 7 mA. A baseband DC-biased optical orthogonal frequency division multiplexing (DCO-OFDM) signal with a peak-to-peak voltage of 1 V was generated using an arbitrary waveform generator (AWG, Keysight M8195A) operating at a sampling rate of 32 GSa/s. The 1550 nm source, in contrast, required a higher bias current of 300 mA at 1.5 V. Due to the AWG's output limitation, a medium-power amplifier (Mini-Circuits ZHL-4240W+) was employed prior to the bias-tee to amplify the DCO-OFDM signal for the 1550 nm source. In both cases, the RF signal was combined with the DC bias using a bias-tee (Mini-Circuits ZFBT-4R2GW+), enabling direct intensity modulation of the optical sources. The modulated light is collimated using a fiber-coupled collimator (Thorlabs F280PC-C), forming a Gaussian beam with a diameter of 3 mm. However, the dimensions of the metasurface are on the order of 100 μm, so a plano-convex lens (Thorlabs LA1608-C-ML, $f = 75$ mm, 1-inch diameter) is

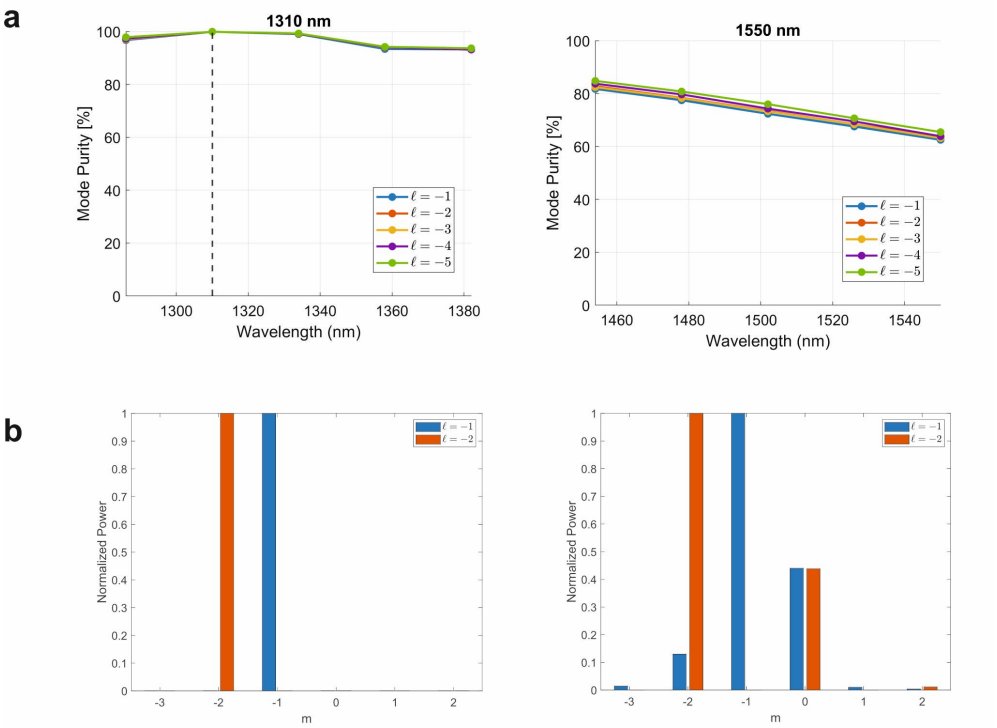

Fig. S3 Simulated performance for negative OAM modes. a, Broadband performance across a 100 nm range, Left: broadband response around the design wavelength of 1310 nm, maintaining purity above 90% across a 100-nm span. Right: off-design operation from 1450 nm to 1550 nm, where the purity gradually decreases from 80% to 60%. **b**, OAM power spectrum for $\ell = -1$ and $\ell = -2$ at 1310 nm (left) and 1550 nm (right)

used to tightly focus the beam on the metasurface. The metasurface is mounted on a 3D nanopositioning stage to facilitate precise alignment. Depending on the pattern encoded on the metasurface, the incident Gaussian beam is converted into an OAM mode of order $l = +1$ or $l = +2$.

To maintain beam collimation through the free-space optical channel, a second aspheric lens (Thorlabs ASL10142M-C, $f = 79$ mm, 1-inch diameter) is used after the metasurface to re-collimate the beam to 3 mm size. The OAM-modulated beam then propagates through a 1-meter line-of-sight optical wireless communication (OWC) link.

On the receiver side, an SLM is programmed with a helical phase pattern to decode a specific OAM mode. When the SLM is configured with a topological charge $m = -l$, where l represents the order of the incident OAM beam, the imposed phase cancels the helical wavefront, thereby converting the beam back into a fundamental Gaussian profile. This transformation facilitates efficient coupling into a single-mode fiber (SMF) using a fiber collimator (Thorlabs F280PC-C). In contrast, beams with non-matching topological charges ($m \neq -l$) maintain their helical structure and are effectively rejected by the spatial filtering characteristics of the SMF.

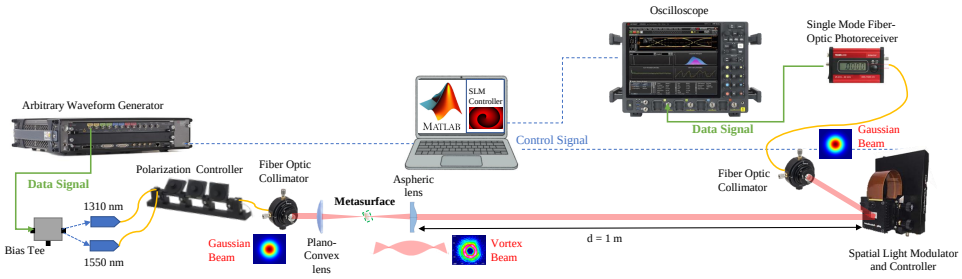

Fig. S4 Schematic of the complete end-to-end metasurface-enabled OAM-based optical wireless communication (OWC) system. The transmitter section (left) includes either a 1310 nm vertical-cavity surface-emitting laser (VCSEL) or a 1550 nm Fabry–Perot laser, both directly modulated by a direct current-biased optical orthogonal frequency division multiplexing (DCO-OFDM) signal. The modulation signal is generated by an arbitrary waveform generator (AWG) and applied via a bias-tee. The modulated light is collimated and precisely focused onto a chip-scale metasurface, which transforms the incident Gaussian beam into a desired OAM mode (l=1 or l=2). A subsequent aspheric lens recollimates the OAM beam for free-space propagation across a 1-meter free-space link. The receiver section (right) employs a spatial light modulator (SLM) programmed with a conjugate helical phase pattern (m=$-l$) to decode the specific OAM mode, converting it back into a fundamental Gaussian profile. This decoded beam is then efficiently coupled into a single-mode fiber (SMF) via a fiber collimator and detected by a single-mode fiber-coupled photoreceiver.

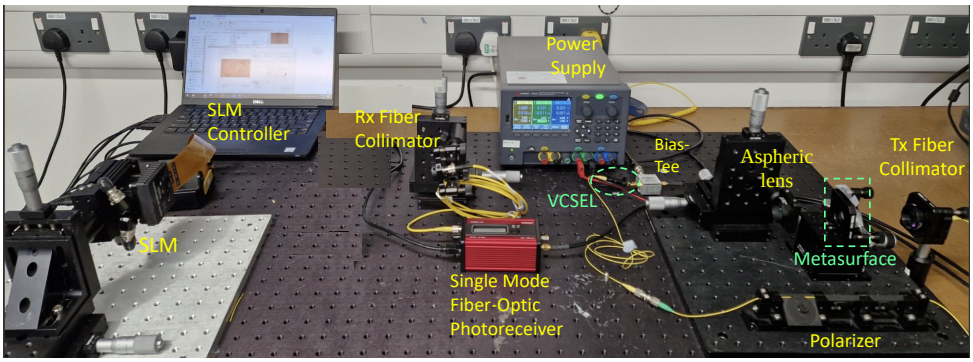

Fig. S5 Photograph of the experimental setup for the metasurface-enabled orbital angular momentum (OAM)-based optical wireless communication (OWC) system. The setup features the transmitter (Tx), which utilizes either an Optilab VCSEL-1310-SM or a Thorlabs LPSC-1550-FC. Key optical components visible include collimators, lenses, and a spatial light modulator (SLM). The metasurface is mounted on a 3D nanostage, and the single-mode fiber-coupled receiver is connected to a collimator at the receiver (Rx) side.

Precise alignment of both the metasurface and SLM is essential to ensure accurate OAM encoding and decoding. In addition, proper alignment of the transformed Gaussian beam with the optical axis of the fiber collimator is critical for maximizing coupling efficiency and minimizing insertion loss. To achieve fine alignment, the fiber collimator is mounted on a three-axis kinematic mount integrated with a high-resolution XYZ translation stage. This configuration provides six degrees of freedom,

enabling sub-micron positional and angular adjustments to optimize beam coupling into the fiber core. The collimator output is connected to the optical input of a single-mode fiber-coupled photoreceiver using a 2-meter single-mode fiber patch cable (Thorlabs P1-SMF28EAR-2), featuring a 10 µm core diameter.

The received optical signal is converted into an electrical signal by a high-speed fiber-coupled photoreceiver (Thorlabs RXM42AF), which contains an indium gallium arsenide (InGaAs) positive-intrinsic-negative (PIN) photodiode, a broadband transimpedance amplifier (TIA), and a variable gain amplifier (VGA) for adaptive signal conditioning. The photoreceiver exhibits broadband responsivity across the 800 nm–1650 nm wavelength range and supports a photodetection bandwidth of up to 42 GHz. A built-in digital display provides real-time monitoring of the average detected photocurrent, which assists with alignment using an unmodulated laser and supports optical power measurements for crosstalk analysis. The resulting analog electrical waveform is digitized by a high-bandwidth oscilloscope (Keysight UXR0104B, 10 GHz) operating at 32 GSa/s, and subsequently transferred to a personal computer for offline signal processing implemented in MATLAB.

S4 Metasurface fabrication

The process flow of the metasurface fabrication is explained in Fig. S6.

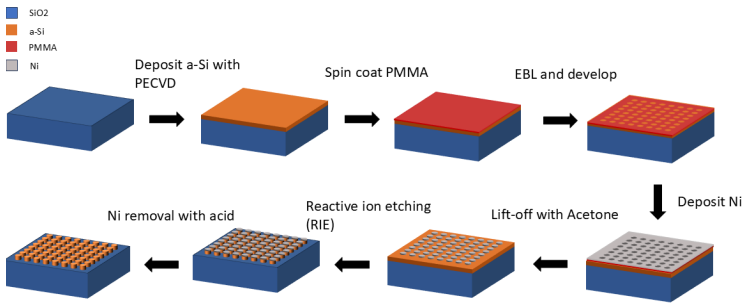

Fig. S6 Process flow for the fabrication of amorphous silicon metasurfaces. The process includes film deposition, lithographic patterning, and reactive ion etching steps.

S5 Digital Signal Processing (DSP)

The DCO-OFDM waveform used in the system is generated using a 1024-point inverse fast Fourier transform (IFFT), with Hermitian symmetry to ensure real-valued time-domain signals. A cyclic prefix (CP) of 15 samples is appended to each OFDM symbol to combat inter-symbol interference. Bit and power loading across the $N_{SC} = 511$ data subcarriers is performed using the Hughes–Hartogs algorithm [17], based on channel signal-to-noise ratio (SNR) estimates. Figure S7 and S8 illustrate the bit and power loading applied for different adaptive iterations of different target BER

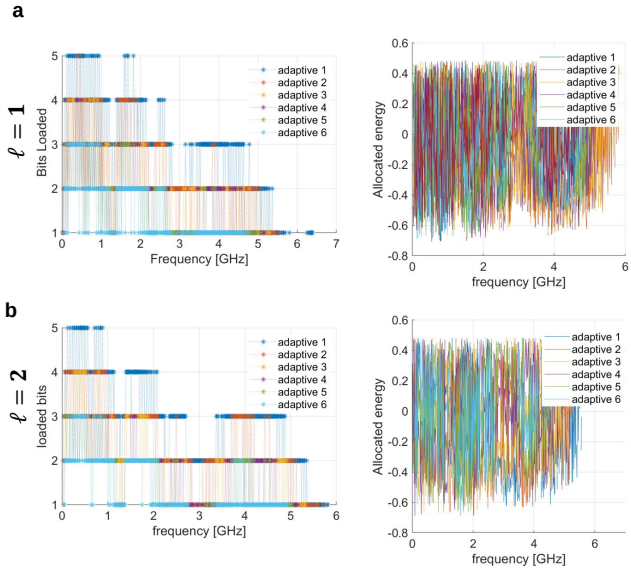

Fig. S7 Experimentally measured bit and power loading at 1310 nm. a, Results for OAM mode $\ell = 1$. **b**, Results for OAM mode $\ell = 2$.

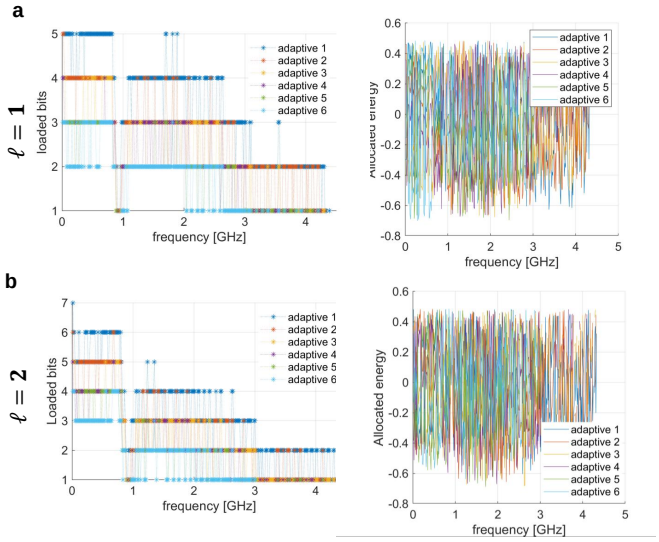

Fig. S8 Experimentally measured bit and power loading at 1550 nm. a, Results for OAM mode $\ell = 1$. **b**, Results for OAM mode $\ell = 2$.

for 1310 nm and 1550 nm. The DCO-OFDM either used binary phase shift keying (BPSK) or quadrature amplitude modulation (QAM). The QAM modulation order per subcarrier ranges from four (QPSK) up to 1024 (QAM-1024), depending on SNR, and a random bit generator is used to create the input bitstream. The resulting waveform is pulse-shaped using a root-raised cosine filter with a roll-off factor of 0.1 to reduce spectral leakage. At the receiver, the digitized signal undergoes frame synchronization, FFT, single-tap equalization, and QAM symbol demapping. A total of 450 OFDM frames (150 pilot + 300 data) are transmitted per experiment to evaluate the bit error rate (BER) performance [18, 19].

References

[1] Wang, J., Yang, J.-Y., Fazal, I.M., Ahmed, N., Yan, Y., Huang, H., Ren, Y., Yue, Y., Dolinar, S., Tur, M., *et al.*: Terabit free-space data transmission employing orbital angular momentum multiplexing. Nature photonics **6**(7), 488–496 (2012) https://doi.org/10.1038/nphoton.2012.138

[2] Yu, Y., Xu, M., Pu, M., Ding, J., Chen, S., Zhang, Y., Zhou, M., Guo, Y., Li, X., Ma, X., *et al.*: Demonstration of 120 Gbit/s turbulence-resilient coherent optical communication employing cylindrical vector beam multiplexing. Optics Express **31**(25), 42165–42175 (2023)

[3] Ren, Y., Wang, Z., Xie, G., Li, L., Cao, Y., Liu, C., Liao, P., Yan, Y., Ahmed, N., Zhao, Z., *et al.*: Free-space optical communications using orbital-angular-momentum multiplexing combined with MIMO-based spatial multiplexing. Optics letters **40**(18), 4210–4213 (2015)

[4] Jurado-Navas, A., Tatarczak, A., Lu, X., Olmos, J.J.V., Garrido-Balsells, J.M., Monroy, I.T.: 850-nm hybrid fiber/free-space optical communications using orbital angular momentum modes. Optics express **23**(26), 33721–33732 (2015) https://doi.org/10.1364/OE.23.033721

[5] Nouri, M., Shahoie, H., LaFave, T., Ashrafi, S., MacFarlane, D.: Orbital angular momentum multiplexing using low-cost vcsels for datacenter applications. Frontiers in Optics 2016, 5–5 (2016) https://doi.org/10.1364/FIO.2016.FW5D.5

[6] Fazal, I.M., Ahmed, N., Wang, J., Yang, J.-Y., Yan, Y., Shamee, B., Huang, H., Yue, Y., Dolinar, S., Tur, M., *et al.*: 2 Tbit/s free-space data transmission on two orthogonal orbital-angular-momentum beams each carrying 25 WDM channels. Optics letters **37**(22), 4753–4755 (2012)

[7] Zhu, Y., Zou, K., Zheng, Z., Zhang, F.: 1 $\lambda\times$ 1.44 tb/s free-space IM-DD transmission employing OAM multiplexing and PDM. Optics Express **24**(4), 3967–3980 (2016) https://doi.org/10.1364/OE.24.003967

[8] Wang, A., Zhu, L., Deng, M., Lu, B., Guo, X.: Experimental demonstration of OAM-based transmitter mode diversity data transmission under atmosphere

turbulence. Optics Express **29**(9), 13171–13182 (2021)

[9] Shi, J., Fang, X., Niu, W., Li, K., Xu, Z., Meng, W., Hu, J., Su, H., Li, D., Ma, Y., *et al.*: 800 Gbps visible light communication system employing WDM and OAM multiplexing. In: 2022 20th International Conference on Optical Communications and Networks (ICOCN), pp. 1–3 (2022). IEEE

[10] Tan, H., Deng, J., Zhao, R., Wu, X., Li, G., Liu, K., Chen, Y., Zhu, S., Wang, X., Jen, A.K.Y., Zhang, X., Yuan, X.: A free-space orbital angular momentum multiplexing communication system based on a metasurface. Laser & Photonics Reviews **13**(6), 1800278 (2019) https://doi.org/10.1002/lpor.201800278

[11] Xie, Z., He, Y., Wang, X., Wu, H., Li, C., Ye, H., Liu, J., Li, Y., Yang, Y., Fan, D., Chen, S.: Phase off-axis modulation metasurface for orbital angular momentum mode multiplexing/demultiplexing. Journal of Lightwave Technology **41**(2), 540–546 (2023) https://doi.org/10.1109/JLT.2022.3218687

[12] Wang, X., Wang, C., Cheng, M., Yang, B., Xie, Z., He, Y., Xiao, J., Ye, H., Li, Y., Fan, D., Chen, S.: Broadband structured light multiplexing with dielectric meta-optics. Journal of Lightwave Technology **39**(9), 2830–2836 (2021) https://doi.org/10.1109/JLT.2021.3064560

[13] Ren, Y., Li, L., Wang, Z., Kamali, S.M., Arbabi, E., Arbabi, A., Zhao, Z., Xie, G., Cao, Y., Ahmed, N., Yan, Y., Liu, C., Willner, A.J., Ashrafi, S., Tur, M., Faraon, A., Willner, A.E.: Orbital angular momentum-based space division multiplexing for high-capacity underwater optical communications. Scientific Reports **6**, 33306 (2016) https://doi.org/10.1038/srep33306

[14] Song, H., Su, X., Song, H., Zhang, R., Zhao, Z., Liu, C., Pang, K., Hu, N., Almaiman, A., Zach, S., *et al.*: Simultaneous turbulence mitigation and mode demultiplexing using one mplc in a two-mode 200-Gbit/s free-space OAM-multiplexed link. In: Optical Fiber Communication Conference, pp. 1–3 (2020). Optica Publishing Group

[15] Wu, Y., al.: Tbps wide-field parallel optical wireless communications based on a metasurface beam splitter. Nature Communications **15**(1), 7744 (2024) https://doi.org/10.1038/s41467-024-28228-9

[16] Cai, X., Wang, J., Strain, M.J., Johnson-Morris, B., Zhu, J., Sorel, M., O'Brien, J.L., Thompson, M.G., Yu, S.: Integrated compact optical vortex beam emitters. Science **338**(6105), 363–366 (2012) https://doi.org/10.1126/science.1226528

[17] Hughes-Hartogs, D.: Ensemble modem structure for imperfect transmission media (1989)

[18] Kazemi, H., Osahon, I.N.O., Jr., N.L., Titkov, I., Ledentsov, N., Haas, H.: Achieving 70 Gb/s over a VCSEL-based optical wireless link using a multi-mode

fiber-coupled receiver (2025) arXiv:2506.18864 [eess.SP]

[19] Chen, C., Das, S., Videv, S., Sparks, A., Babadi, S., Krishnamoorthy, A., Lee, C., Grieder, D., Hartnett, K., Rudy, P., Raring, J., Najafi, M., Papanikolaou, V.K., Schober, R., Haas, H.: 100 Gbps indoor access and 4.8 Gbps outdoor point-to-point LiFi transmission systems using laser-based light sources. Journal of Lightwave Technology **42**(12), 4146–4157 (2024) https://doi.org/10.1109/JLT.2024.3400192